Journal of Theoretical Biology 266 (2010) 614–624

Contents lists available at ScienceDirect

Journal of Theoretical Biology

journal homepage: www.elsevier.com/locate/yjtbi

A multiscale, spatially distributed model of asthmatic airway hyper-responsiveness

Antonio Z. Politi [a,1], Graham M. Donovan [b,*,1], Merryn H. Tawhai [b], Michael J. Sanderson [c], Anne-Marie Lauzon [d], Jason H.T. Bates [e], James Sneyd [a]

[a] Department of Mathematics, University of Auckland, Private Bag 92019, Auckland Mail Centre, Auckland 1142, New Zealand
[b] Auckland Bioengineering Institute, University of Auckland, Private Bag 92019, Auckland Mail Centre, Auckland 1142, New Zealand
[c] Department of Physiology, University of Massachusetts Medical School, Worcester, MA 01655, USA
[d] Department of Medicine, Meakins-Christie Laboratories, McGill University, Montreal, Canada
[e] Vermont Lung Center, Fletcher Allen Health Care, Department of Medicine, University of Vermont, Burlington, VT 05405, USA

ARTICLE INFO

Article history:
Received 1 February 2010
Received in revised form
26 July 2010
Accepted 26 July 2010
Available online 4 August 2010

Keywords:
Crossbridge
Calcium
Tethering
Smooth muscle cells
Actin–myosin

ABSTRACT

We present a multiscale, spatially distributed model of lung and airway behaviour with the goal of furthering the understanding of airway hyper-responsiveness and asthma. The model provides an initial computational framework for linking events at the cellular and molecular levels, such as Ca^{2+} and crossbridge dynamics, to events at the level of the entire organ. At the organ level, parenchymal tissue is modelled using a continuum approach as a compressible, hyperelastic material in three dimensions, with expansion and recoil of lung tissue due to tidal breathing. The governing equations of finite elasticity deformation are solved using a finite element method. The airway tree is embedded in this tissue, where each airway is modelled with its own airway wall, smooth muscle and surrounding parenchyma. The tissue model is then linked to models of the crossbridge mechanics and their control by Ca^{2+} dynamics, thus providing a link to molecular and cellular mechanisms in airway smooth muscle cells. By incorporating and coupling the models at these scales, we obtain a detailed, computational multiscale model incorporating important physiological phenomena associated with asthma.

1. Introduction

It is estimated that 300 million people worldwide suffer from asthma (Braman, 2006), a disease characterised by the emergent phenomena of airway hyper-responsiveness (AHR) and airway hyper-sensitivity. In AHR, the airways contract too severely; in airway hyper-sensitivity, they contract too readily. In particular, AHR is of primary interest because it is associated with the majority of asthmatic mortality and morbidity (Sterk and Bel, 1989). While the exact mechanisms involved are still an area of active research, it is believed that the role of airway smooth muscle contraction is critical in this excessive airway narrowing (Krishnan et al., 2008).

This work is part of a larger effort to create a comprehensive multiscale model of asthmatic AHR. The ultimate goal of the project is to develop a model encompassing and linking the molecular, cellular, tissue and organ scales. In this work, we present an initial computational framework for this multiscale model, focusing on how the organ level model can be linked to the tissue level model, and also on how molecular and cellular models can be included, resulting in a multiscale model that spans the entire range of spatial scales.

2. Multiscale model

Our approach to creating a multiscale model of asthmatic AHR involves joining models at four spatial scales: organ, tissue, molecule and cell. At the organ level, a continuum mechanics approach is employed to solve the mechanical deformations of the lung due to breathing and gravity (Section 2.1). The organ-level model provides the boundary pressures and local elastic properties of the parenchyma used as model inputs in the tissue-level model (Section 2.2), describing the behaviour of individual airways. The airway lumen radii computed at the tissue-level depend on the coupling with the organ level model, the nonlinear properties of the airway wall, and the active force generated by the airway *smooth muscle cells* (SMC) at the cellular level. The active force is modelled according to sliding filament theory, and controlled by intracellular Ca^{2+} dynamics, which is determined by the degree of external stimulation (Section 2.3). The stimulation is provided by an introduced agonist, triggering Ca^{2+} release

* Corresponding author.
E-mail address: g.donovan@auckland.ac.nz (G.M. Donovan).
[1] Contributed equally to this work.

0022-5193/$ - see front matter © 2010 Elsevier Ltd. All rights reserved.
doi:10.1016/j.jtbi.2010.07.032

at the molecular level and thus airway contraction. This introduced agonist mimics bronchial challenge, a standard clinical practice in the study of asthma (Cockcroft et al., 2001). The crossbridge model has already been treated in detail by Wang et al. (2008), while, for simplicity, we shall assume a piecewise constant Ca^{2+} concentration. We are currently developing a detailed model of Ca^{2+} dynamics in SMC, accounting for Ca^{2+} oscillations and frequency encoding of the stimulus (Perez and Sanderson, 2005), and this model can be easily incorporated into the framework described here.

2.1. Organ-level model

The human lung contains a bronchial airway tree with an asymmetric branching structure beginning at the trachea and descending to more than 30,000 distal terminal bronchioles no more than 0.6 mm in diameter, with a total of 27 airway orders, on average (Horsfield et al., 1971). The bronchial airways do not take part in gas exchange. The airway wall consists of a layer of airway smooth muscle, as well as an inner layer of mucosal and epithelial cells, all surrounding the airway lumen. The terminal bronchioles, the smallest and most peripheral conducting airways, connect with respiratory bronchioles, alveolar ducts, and alveolar sacs, each of which has walls fully or partially comprising alveoli. The alveoli are the site of respiratory gas exchange. Along with the corresponding pulmonary vasculature, this complex structure fills the volume of the lungs.

We begin by considering an arbitrary three-dimensional unit of lung tissue. While the methods we employ are agnostic to the tissue geometry, and can in fact be applied to anatomically-correct, patient-specific geometries (Tawhai et al., 2006, 2009), for simplicity at this stage we consider a smaller tissue unit which can be thought of as a spatial segment of the larger problem; see Fig. 1. The location of the tissue unit is not explicitly anatomically defined, but may be thought of as being away from the surface of the lung, in the centre of the gravitational field, and away from inter-lobar fissures. This tissue unit is initially uniform pulmonary parenchyma, within which the conducting bronchial tree is embedded. All structures aside from the conducting bronchial tree, including the acini and vasculature, are included in the parenchymal continuum. The conducting airway tree can thus be thought of as being embedded, or, alternately, as being suspended in a fibre network (Weibel, 1984). The conducting bronchial tree in the tissue unit may also be considered as a terminal subtree of the entire lung tree: it contains 90 airways ranging from distal terminal bronchioles at order 1 up to order 8, but no higher-order airways.

The airway tree geometry is generated throughout the tissue unit by a morphometrically-accurate, asymmetric-branching, 3D tree-generating algorithm (Tawhai et al., 2004). Because of the number of airways involved in computing a complete lung, we make several simplifying assumptions with regard to the airway tree in order to achieve computational feasibility. While perhaps not strictly necessary for simulating the smaller tissue unit, the computational complexity concerns are essential for scaling up to the complete lung geometry. For each airway segment, we assume that the airway is radially symmetric and longitudinally stiff. Thus, while they are distributed in a 3D tissue unit, each airway segment is essentially 1D. The change in length of the airway is computed during simulated breathing, however, the radial airway mechanics are assumed to be independent of changes in airway length during tidal breathing.

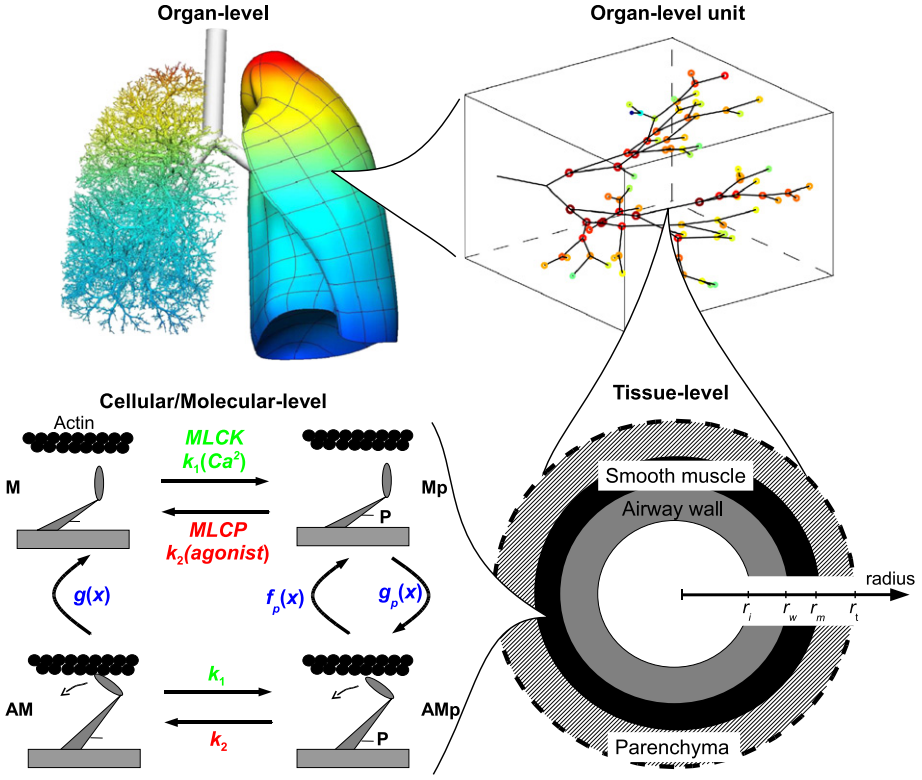

Fig. 1. Schematic of multiscale interactions. Upper left panel: complete anatomically-accurate organ-level model, with parenchymal tissue elements displayed in the left lung and the embedded airway tree in the right. Upper right panel: organ-level tissue unit with 90 embedded airway segments. The circles at the airway tree bifurcations represent the radii computed at the tissue level. Lower right panel: in the tissue level, each airway segment is modelled as a cylinder. We consider three layers: airway wall, smooth muscle cells, and a parenchymal layer. Lower left panel: cellular/molecular level. Phosphorylation of myosin (M to Mp) enables binding to actin (A). Force is generated by the attached populations, AM and AMp. Phosphorylation is controlled by several stimuli that increase Ca^{2+} release which in turn activates MLCK, whereas dephosphorylation is controlled by MLCP, which itself can be regulated by agonists.

The tissue unit is subject to expansion and recoil to simulate the breathing process, as well as the effects of gravity. The tissue mechanics are considered in a finite deformation elasticity framework, in which the pulmonary parenchyma is modelled as a compressible, hyperelastic material. This material is assumed to be initially isotropic, with a strain energy density function given by

$$W(E) = \frac{C}{2}\exp(\alpha J_1^2 + \beta J_2) \tag{1}$$

due to Fung et al. (1978). Here J_1 and J_2 are the first and second invariants of the Green strain tensor E, given by $J_1 = \mathrm{Tr}(E)$ and $J_2 = -\frac{1}{2}[\mathrm{Tr}(E^2) - (\mathrm{Tr}E)^2]$. The parameter values are taken to be $\alpha = 0.433$, $\beta = -0.611$, and $C = 2500\,\mathrm{Pa}$. The value of the C coefficient is chosen such that uniform inflation of the tissue to volumes equivalent to functional residual capacity (FRC) and total lung capacity (TLC) requires physiologically reasonable expansion pressures. The equivalent linear bulk and shear moduli obtained with this material law are proportional to the inflation pressure; the pressure–volume, and shear modulus–stress relationships for this model have been previously published (Tawhai et al., 2009). There are many other models in the literature which could be used to describe parenchymal mechanics, some of which include phenomena which the strain energy approach fails to capture—see Section 4. In the spatially restricted tissue unit, a number of these alternative models might be employed; however, it is with an eye toward the next stage of model development, wherein full patient-specific geometries obtained from imaging data will be used, that we have selected the strain energy approach. In this case, from a computational, finite-element perspective, it is the best available model.

The boundary conditions on the tissue unit are set to provide a prescribed change in volume via uniform expansion/contraction of gravitationally deformed tissue to simulate the breathing process. The tissue begins at a reference state, referred to as reference volume (V_{ref}), with zero strain and is initially inflated by a factor of two in volume to FRC. A body force with direction and magnitude of gravity is added to the system at FRC. From FRC, tidal breathing involves a 20% increase in volume, while TLC is a doubling in volume from FRC. Thus TLC is a total four-fold volumetric increase from the reference state. Note that our reference state is not physiological residual volume, but that the operational regime of the lung is far away from zero stress–zero strain. Because the stress–strain curve has small slope in this range, our reference state is a reasonable approximation to the true physiological zero stress–zero strain state.

The finite elasticity governing equations are then solved via a finite element method. As the lung tissue unit undergoes expansion or recoil due to breathing, pressure is exerted on the embedded airway tree structure and the material properties around the airway change. At each point in the tree, the pressure and local material properties at the airway location are calculated from the organ-level continuum model and used as inputs in the tissue-level model. Note that because the expansion is anisotropic, the linearisation depends on airway orientation—see Section S.II in the supplementary material for more details. With the airway radius data from the tissue-level model (coupled to the cellular and molecular scale models), described in the following sections, and the airway tree geometry data from the organ-level model, we have a complete description of the behaviour of the airway tree.

2.2. Tissue-level model

In the tissue-level model, each airway segment, modelled as a 1D line in the previous section, is now represented as a cylinder of fixed length. We consider three layers: the airway wall, a smooth muscle cell layer, and a parenchymal layer. It has previously been shown that when considering dynamic airway contraction it is necessary to consider both airway wall properties, including significant stiffness, and elastic parenchymal tethering forces in order to obtain good agreement with experimental data (Bates and Lauzon, 2007). The lower-right panel of Fig. 1 is a simple schematic of the layers included in the model. The circles at each airway bifurcation in the upper-right panel of Fig. 1 represent the airway radius in the segment above that bifurcation.

Each airway segment is classified according to *Horsfield order* (Horsfield et al., 1971), and the properties of the airway wall depend on airway order (Lambert et al., 1982; Lambert and Wilson, 2005). Initial airway radii are determined only by airway order; all airways of the same order begin with equal radii. For additional details of order-dependent parameters, see supplementary material Section I.

The local parenchymal layer is required to account for the additional tethering force that develops due to local tissue stretch during active airway contraction; the organ-level model provides the boundary pressure and elastic material parameters for this layer. Force balance across all layers determines the size of the airway lumen. In the following, we briefly describe the different elements of the tissue-level model. A detailed derivation of the model is given in the supplementary material. For simplicity, all results assume plane strain and cylindrical symmetry.

2.2.1. Airway wall and smooth muscle

We treat the airway wall and surrounding airway smooth muscle as separate layers—see lower right panel of Fig. 1. The passive properties of the airway wall determine the size of the airway lumen in response to transmural pressure, while the active smooth muscle force generated in the smooth muscle layer contributes to the pressure across the airway wall. Thus the radius r_i of the airway lumen is determined by the transmural pressure P_{tm} across the airway wall

$$P_{tm} = P_i + P_w, \tag{2}$$

where P_i and P_w are the pressures on the luminal and adventitial side of the airway wall, respectively. All surface normal vectors point in the direction of increasing airway radius. The relationship between P_{tm} and r_i is detailed in the supplementary material, Section I. The pressure P_w at the interface between the airway wall and the smooth muscle layer is computed from the pressure exerted by SMC and the parenchymal layer and is then given by

$$P_w = P_m - f\frac{R_m - R_w}{r_s}, \tag{3}$$

where f is the active circumferential stress exerted by the SMC, P_m is the pressure at the SMC-parenchyma interface, $r_s = (r_w + r_m)/2$ is the mean SMC radius, and $Rm - R_w$ is the order dependent SMC layer thickness at $P_{tm} = 0$ (see also supp. mat. Section I). The parameters R_w and R_m are the radii r_w and r_m in the reference configuration, $P_{tm} = 0$. All radii are given in units of mm, and thus the quantity $(R_m - R_w/r_s)$ is dimensionless and f is a stress. Sufficiently large activation of SMC will induce a negative pressure P_w and hence airway contraction.

We assume incompressibility in both the airway wall and SMC layer. Conservation of volume yields a relation between deformed and undeformed radii in these two layers, Eqs. S.4 and S.5 in the supplement. Note that in the absence of smooth muscle force, $f = 0$ and hence $P_{tm} = P_i + P_m$.

The active stress f is computed from the crossbridge model (Wang et al., 2008); it accounts for binding and dissociation of myosin heads to actin and how those rates vary with external

stimulation, contraction velocity, and SMC length (see Section 2.3 and supplement Section III).

2.2.2. Parenchyma

Airway contraction distorts the parenchyma surrounding the airway and increases what is known as *tethering force*, a recoil force opposing airway contraction. We consider for each airway two regions of parenchyma: the parenchymal continuum, in the organ-level model, and a layer of parenchyma local to each airway, located between r_m and r_t. There are no explicit alveoli in the model; they have been absorbed into the parenchyma. The pressure P_t is calculated from the organ-level model, and the local parenchymal layer is used to calculate the local increase in tethering force due to airway constriction yielding the pressure P_m. A decrease in airway radius causes an expansion of the local parenchymal region and hence an increase in tethering force and P_m. Note that the boundary between the local parenchymal layer and the organ-level model at r_t (R_t) will be taken as a far-field condition where $r_t \gg r_m$ ($R_t \gg R_m$) and hence r_t and R_t do not appear explicitly in the final equations. We will also assume that no neighbouring airways exist within the radius of the local parenchyma, so that parenchymal distortion caused by the contraction of one airway does not influence other airways.

For the material law given in Eq. (1), no analytical solutions of parenchymal displacement and stress inside this local layer could be found; we therefore approximate the problem using linear elasticity. Assuming that active contraction causes small displacements of the parenchyma, we linearise the local stress, obtained from the organ-level model, around the actual deformation state. This depends both on the nonlinear material state and airway orientation—see supplement Section II. The linearisation yields a pre-stress and the shear modulus μ describing the local, linear parenchymal layer. These two parameters depend on the actual strain of the parenchymal tissue obtained from the organ-level model. This method intrinsically accounts for the stiffening of the parenchyma for increasing lung volumes and is originally due to Lai-Fook (1979). To account for additional local nonlinear effects caused by airway contraction, we use a second-order phenomenological approximation

$$P_m = 2\mu[\Delta R_m + v(\Delta R_m)^2] + P_t, \tag{4}$$

where

$$\Delta R_m = (\overline{R}_m - r_m)/\overline{R}_m. \tag{5}$$

The linear term comes from the linear elasticity assumption, while the quadratic coefficient $v = 1.5$ has been determined from experimental data (Lai-Fook, 1979). In this equation P_t and μ are obtained from the organ-level model of the parenchymal continuum—important details of this relationship are discussed further in Section 2.2.3. Because the alveoli are included in the parenchymal continuum, alveolar pressure appears implicitly as part of P_t. While in general the unstrained parenchymal radius is constant, the linearisation creates an *implied* linearised unstrained parenchymal radius, denoted $\overline{R}_m$ (see supplement Section II).

In the absence of active force and airway contraction, the pressures at the airway wall, smooth muscle layer, and parenchymal tissue/far-field are all equal: $P_w = P_m = P_t$. Sufficient SMC activation ($f > 0$) causes both inward force on the airway wall so that $P_w < P_m$ and parenchymal tethering force such that $P_m > P_t$.

2.2.3. Parenchymal coupling

The model contains multiple representations of the parenchyma, and the relationship between these regions requires additional description. At the organ scale, the global parenchyma is an anisotropic continuum, as described in Section 2.1. Each individual airway is connected to a local parenchymal layer, which accounts for the increased tethering force caused by airway constriction. It is assumed that only one airway occurs within each local parenchymal layer.

The material properties of the local parenchymal layer are connected to the global parenchymal state at that location, but they are not identical. The local parenchyma is a linear, rather than nonlinear, material, with material parameters determined by linearising the global, organ-level parenchyma at each specific location in both space in time. This process depends upon the local airway orientation because the organ-level material stress is anisotropic, and a single value for the stress is taken by averaging radially (perpendicular to the airway vector). Precise details of this relationship are given in the supplementary material S.II.

2.3. Cellular- and molecular-level models

At the cellular level, airway SMCs are modelled according to the sliding filament theory, and the generated force is calculated using a modified crossbridge model (Wang et al., 2008). This model takes into account both the SMC length and external stimulation; for complete details, see supplement Section III. Binding of myosin to actin, and hence force generation, is controlled by myosin light chain phosphorylation. This is set by the balance between two stimulus-dependent enzymes, myosin light chain kinase (MLCK) and phosphatase (MLCP). Binding of agonists to membrane receptors causes Ca^{2+} release from intracellular stores into the cytoplasm and triggers activation of MLCK (Kamm and Stull, 2001). The MLCP can in turn be inactivated by the presence of other agonists, in a process called Ca^{2+} sensitisation (Somlyo and Somlyo, 2003).

Following Hai and Murphy (1988), we distinguish four states for myosin (see Fig. 1, lower-left panel): two actin-bound states, AM and AM_p, and two free states, M and M_p, where the subscript indicates phosphorylation. It is only the bound states that generate active force. The transition between attached and detached states is modelled according to the sliding filament theory, which has been shown to reproduce several important dynamic properties of SMC (Mijailovich et al., 2000; Wang et al., 2008). Because the attachment and detachment rate constants are functions of the crossbridge displacement x, the amount of attached myosin depends directly on dynamic length changes in the SMC—the velocity of airway contraction and relaxation. The length changes are in turn determined by the coupling to the tissue and organ level models (see supplement Section III).

The SMC force is also set by its overall length. It has been shown that long after a change in SMC length, the isometric force remains below the force obtained at the so-called adapted length (Gunst and Stropp, 1988; Ishida et al., 1990; Wang et al., 2001; Herrera et al., 2005). The relation between isometric force and length is characterised by a force–length curve. To include this in the model, we take the SMC tension as

$$f = f_L f_a, \tag{6}$$

where f_a is the adapted-length tension given by

$$f_a = \kappa \int_{-\infty}^{\infty} x(AM + AM_p)\, dx. \tag{7}$$

Here we have assumed that the crossbridges act as linear springs, and κ characterises the stiffness of the muscle. Furthermore, we assume as in the original work (Hai and Murphy, 1988), that the latch state, AM, exerts the same force as phosphorylated attached myosin, AM_p. We approximate the experimental data with

$$f_L = \sin\left(\frac{\pi r_s}{2 r_{s\max}}\right)^3 \tag{8}$$

for $r_s \leq 2r_{smax}$ and $f_L = 0$ otherwise. Different functional forms can be used without significant impact on the results. We assume that $f_L = 1$ at TLC, so that r_{smax} is the radius at TLC (see Table S.1).

The cellular-level crossbridge model is dependent on a molecular-level Ca^{2+} model. At the current stage, for simplicity, we assume a simple imposed Ca^{2+} concentration: initially constant until agonist application, when a 2-second period linear increase precedes a higher constant level for the duration of the simulation.

2.4. Multi-scale interactions

To solve the multi-scale model at each time step, we perform the following calculations:

- Impose a volume change on the lung and solve the finite elasticity problem. Together with gravity, this yields deformation and stress in the lung.
- At each airway segment, the deformation gradient tensor is used in conjunction with the airway direction vector to compute the radial stress and local shear modulus of the local parenchymal layer, which in turn determines the increase in tethering force.
- The crossbridge model is used to compute the velocity of displacement and force exerted by the SMC.
- The new airway radius is given by force balance of all these factors.

The model contains four separate scales: organ, tissue, cellular and molecular. In addition to the dynamics at each level, the levels are connected as follows. The organ-level model influences the tissue-level model via the cyclic recoil pressure and the local parenchymal material state. The tissue-level model passes information to the cellular-level by way of the macroscopic smooth muscle contraction velocity, which is proportional to the microscopic crossbridge velocity at the cellular level. The cellular model is connected back to the tissue level model both by the contraction velocity and the generated force. The molecular-level imposes the Ca^{2+} concentration due to agonist on the SMCs at the cellular level. These relationships are summarised in Fig. 2.

In order to implement this model computationally, it is important to account for the fact that in certain situations the pressure–radius relationship may become multi-valued, as has been previously suggested by others (Macklem, 1995). This static bistability would normally allow the solution to "jump" instantaneously from one solution to another, but this would not yield correct dynamics; we demonstrate that because of the multiscale coupling in this model, the crossbridge dynamics modulate the transition between stable states such that slow and steady contraction is still seen. See Section 3.3 for additional details.

It is important to note that we do not include one important mechanism which triggers bistability found in Anafi and Wilson (2001) and Venegas et al. (2005), the feedback between flow and airway resistance, whereby tidal volume is maintained during constriction and airways are connected such that constriction on one part of the airway tree must be compensated by a dilation elsewhere. In this model we have neglected airflow and all variation comes from the pressure imposed externally on the airway (P_t), which is independent of all other airways. Neglecting airflow is a significant assumption and is discussed in Section 4.

3. Results

To simulate agonist challenge, we choose to compute a 200 s window with 4-second tidal breathing repeated throughout. A variable timestep algorithm is used, with a minimum timestep of $t = 0.005$ s and a maximum of $t = 0.125$ s. Thus we inflate the tissue from V_{ref} to FRC to initialise the simulation, and then proceed with tidal breathing oscillations and introduce the agonist concentration at $t = 10$ s. The breathing is normal up to this point, when agonist is introduced uniformly to the system and airway contraction begins. The pressure applied on each airway in the embedded tree due to the breathing is calculated from the organ-level, continuum mechanics model, and represented in Fig. 3 for a single breathing cycle. The variation between airways is a result of the spatial distribution of tissue stress (due to the nonlinear material properties), as well as airway orientation relative to the gravitational body force. In fact, the pressure and material property variation obtained within the tissue unit is relatively small compared with expectations for variations across a complete, anatomically-accurate lung geometry. Additional discussion of this spatial variation can be found in Section 3.2.

This applied pressure is supplied to the tissue-level model, which, along with the agonist concentration and parenchymal material properties, determines the airway radii by way of crossbridge dynamics, airway wall mechanics, and local parenchymal distortion. The (normalised) mean time courses of these radii, with agonist introduced at $t = 10$ s, are given in Fig. 4. The final conducting airway radii, measured at the final return to FRC, vary from approximately 38.2% to 59.8% of their initial values; the mean is 42.6%. Intra-order heterogeneity depends upon gravity, nonlinear tissue expansion, and airway orientation; inter-order heterogeneity is further influenced by order-dependent airway wall mechanics. Further discussion of this point can be found in Section 3.2.

Airway contraction causes distortion in the surrounding parenchyma, and the resulting parenchymal tethering force is incorporated into the force-balance calculation. The contribution of this increase in tethering force, when compared with the cyclic recoil pressure (from the organ-level only), is illustrated in Fig. 5 for a single, sample airway in the simulation. According to the model the increase in the tethering force is of the same order of magnitude as the applied pressure, and so contributes considerably in determining the airway radius during SMC activation. The increase in parenchymal tethering pressure obtained here is qualitatively consistent with previously obtained experimental results (Bates et al., 1994).

The final spatial distributions of P_t and the airway contraction ratio $r_i/r_i(0)$ are given for each airway segment in the tissue unit in Fig. 6. The circle radii correspond to airway radii, while the colour indicates the cyclic recoil pressure and airway cross-sectional area contraction ratio, left and right, respectively.

One phenomenon observed in this multiscale model is the reduction of crossbridge force generation due to macroscopic tidal breathing oscillations, an effect previously demonstrated by

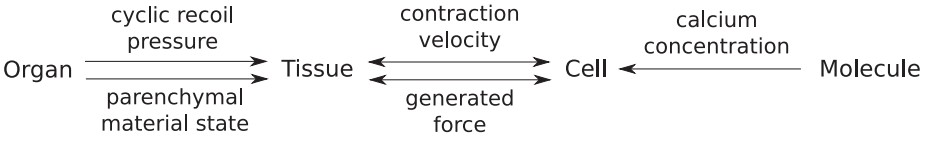

Fig. 2. Diagram of multiscale interactions.

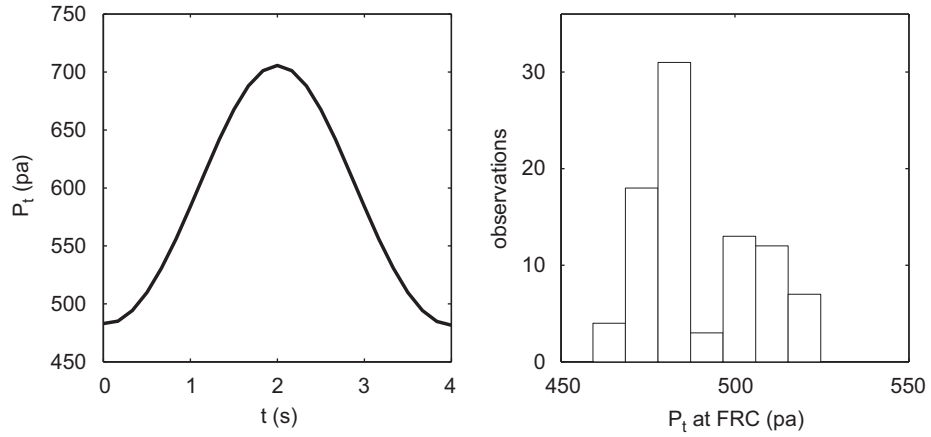

Fig. 3. Cyclical recoil pressure. Left panel: mean time course of the external pressure for all simulated airways over a single breath. The right panel is a histogram of the pressure distribution at FRC.

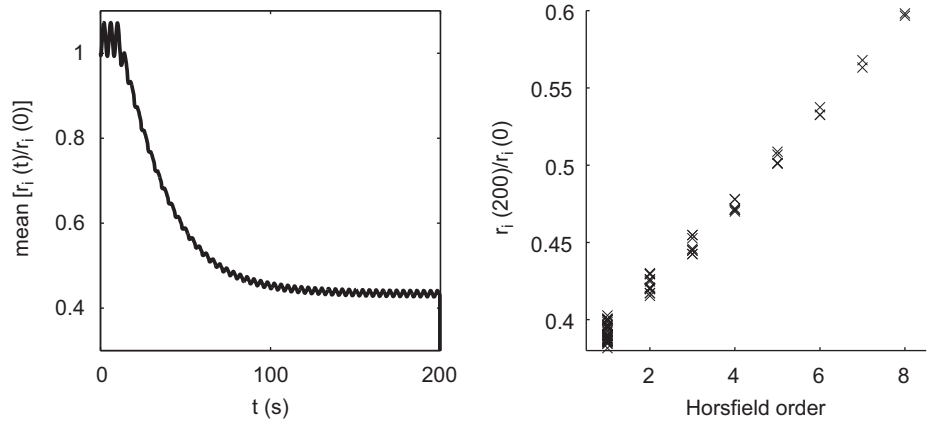

Fig. 4. Conducting airway radii. Left panel: mean time course of the rescaled radius $r_i/r_i(0)$ for all simulated airways. The distribution around this mean is represented in the right panel at end of the final inspiration, $t=200$ s, with the rescaled radius on the vertical axis and the airway order on the horizontal. Contraction is initiated by increasing $[Ca^{2+}]$ from $c=0.05$ to 0.65 μM and agonist from 0 to 1 (a.u.) at $t=10$ s.

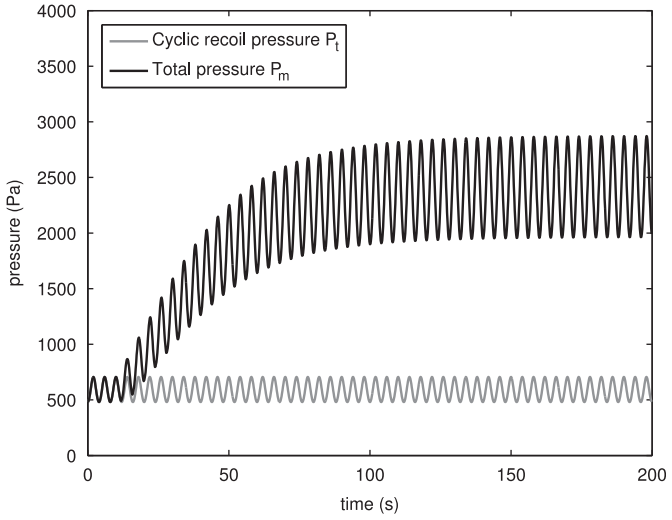

Fig. 5. Cyclical recoil pressure P_t and total pressure P_m, including tethering pressure, for a single, sample airway. Agonist introduced at $t=10$ s.

others (i.e. Latourelle et al., 2002; Winkler and Venegas, 2007; Brown et al., 1994). Because of the coupling between macroscopic and microscopic velocities, macroscopic tidal oscillations create a microscopic velocity which prevent actin–myosin binding and cause force reduction. The force reduction then leads to an increase in airway radius. To measure this effect, we simulate our multiscale model with averaged external organ-level pressure and material properties and compare with the results for tidal breathing during agonist challenge. The results of these simulations are given in Fig. 7, with the normalised volume of the airway tree plotted against time in each situation. The grey curve is in the case of tidal breathing, the black, solid curve is in the static case without tidal breathing (with static properties equal to the mean tidal breathing properties) and the black, dashed curve is the time average of the grey curve. Force reduction due to tidal breathing causes the difference between black dashed and solid curves. While several studies have found much larger dilations than seen here (cf. Latourelle et al., 2002; Winkler and Venegas, 2007; Brown et al., 1994; Shen et al., 1997), more recent work in intact airways suggests that, *in situ*, the dilation may in fact be very small (LaPrad et al., 2010). The magnitude of the effect and the factors influencing it within the multiscale model are discussed in the following section.

3.1. Relative influence of oscillations on constriction

While force reduction caused by breathing oscillation is a phenomenon fundamentally due to the dynamics of the included crossbridge model, the magnitude of dilation is determined not only by the crossbridge model, but also the incorporated models

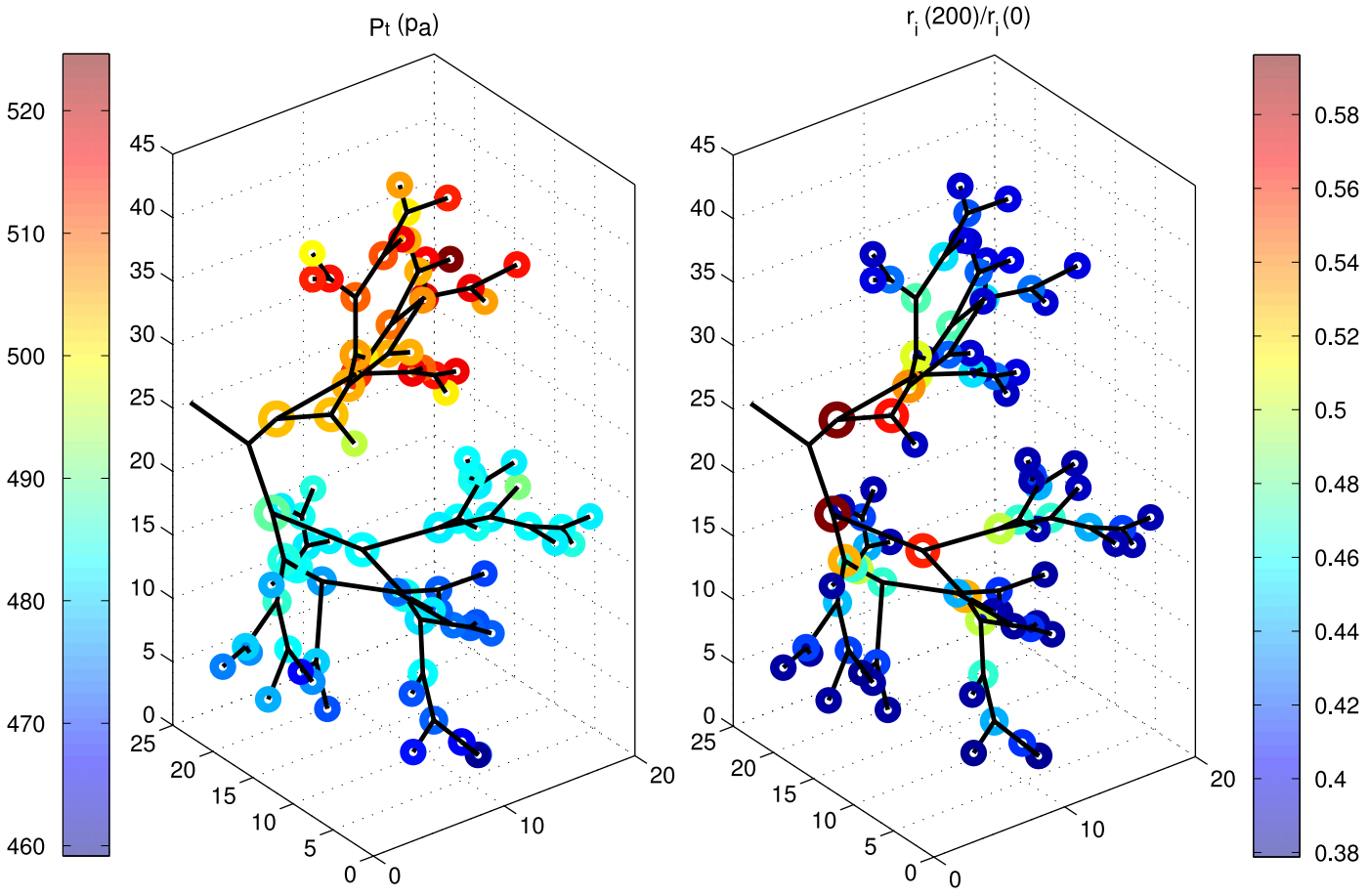

Fig. 6. Final spatial distributions at each airway segment in the tissue unit. Left panel: external cyclic recoil pressure P_t in (Pa). Right panel: airway cross-sectional area contraction ratio $r_i/r_i(0)$. In each plot, the circles at each junction represent the airway radius in that segment and the colour the indicated quantity.

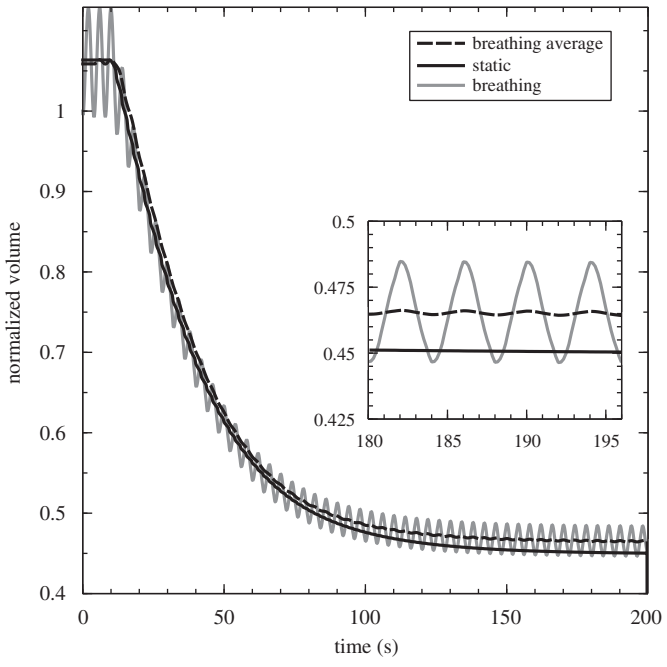

Fig. 7. Normalised volume of simulated airway tree for oscillatory breathing behaviour (grey), static average pressure and material properties (black, solid), and the time-average of the breathing behaviour (black, dashed). The difference between the static solution and the breathing average indicates the crossbridge force reduction due to tidal breathing.

at other scales. A greater degree of dilation can be obtained by altering the model parameters in various ways; however, most parameters have been previously determined in order to agree with experimental data and obtain other behaviours. For example, altering the crossbridge cycling rates can achieve much larger dilations, but potentially at the cost of the experimental agreement obtained in Wang et al. (2008).

In order to assess the influence of interactions between multiple scales on the overall radius increase due to oscillations, we have performed a sensitivity analysis. We systematically varied 16 model parameters and analysed their influence on this particular outcome (Fig. 8). Unsurprisingly, the crossbridge attachment and detachment rate parameters f_{p1} and g_{p1} have the largest influence. However, significant impact is also obtained by increasing the maximum isometric smooth muscle force κ or the phosphorylation rate k_{on2}. The other parameters examined have minimal influence.

It is also possible that this level radius increase is in fact the appropriate degree for the situation under consideration here. Potentially important differences with previous studies include the order of the airways under consideration, the size of the tidal oscillations, the state of health of the tissue, the observed timescales and the severity of the imposed constriction. For example, Brown et al. (1994) considers deep inspirations rather than tidal oscillations; Winkler and Venegas (2007) consider the problem as coupled with airway closure; and the largest force dilations in Latourelle et al. (2002) occur under conditions of larger pressure oscillations (ΔP of 500 Pa compared to approx. 150 Pa here) and on much longer timescales. However, it should

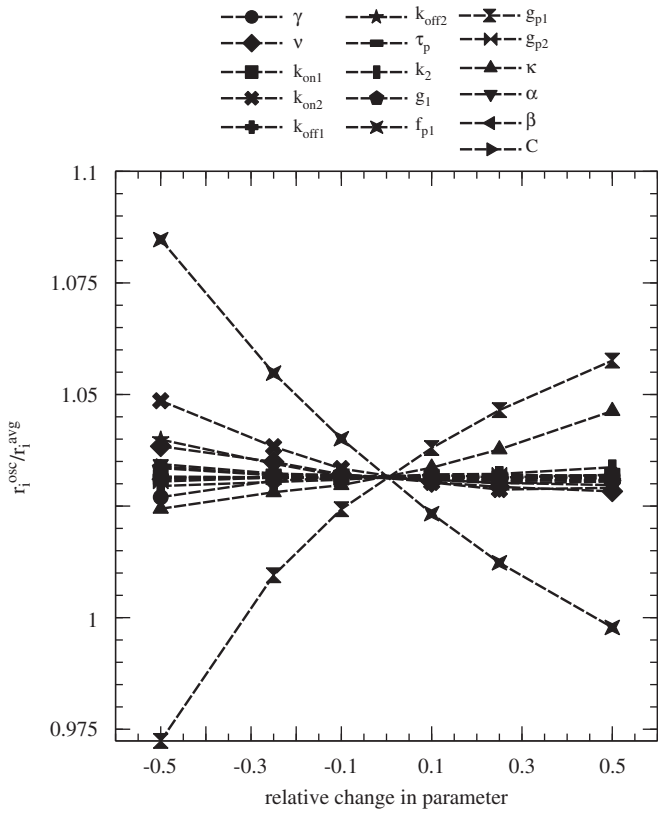

Fig. 8. Sensitivity analysis of volume increase due to tidal breathing oscillations. 16 model parameters are evaluated for their impact on the magnitude of the final volume increase.

be noted that smaller values of ΔP in Latourelle et al. (2002) still yielded greater dilation than seen here. Another confounding aspect in comparing studies is the mean value of the oscillations, rather than only the amplitude; for example, the *in vivo* results of Shen et al. (1997) use tidal oscillations above, rather than about, a baseline value, such that by increasing ΔP the mean value of P is correspondingly increased. It may also be that multiscale interactions have a significant quantitative influence on this effect (i.e. Bates, 2010). In fact, it has been suggested by more recent experimental work (LaPrad et al., 2010) that *in situ* airway behaviour, rather than isolated ASM, shows little or no effect, and this is attributed to interactions between different scales.

For comparison, we also simulated the force reduction in the model in isolated ASM, without coupling to the models at other scales. For 5%, 10% and 20% length oscillations about fixed mean (with γ as for an upper, Horsfield order 27 airway), force reduction versus isometric activation measured 3.49%, 6.93% and 15.22%, respectively. Though fixed oscillations of this form are not directly comparable to the multiscale case, this suggests that interactions between scales are responsible for a significant reduction in the observed magnitude of dilation.

3.2. Spatial heterogeneity

The simulation results exhibit spatial heterogeneity, both intra- and inter-order, and this is due to four effects included in the model. Intra-order heterogeneity is caused by gravity, nonlinear tissue expansion (Section 2.1), and varying airway orientation (Section 2.2.3). Additional inter-order heterogeneity is caused by order-dependent airway wall parameters (Section 2.2).

For intra-order heterogeneity, the effects of gravity and airway orientation may be easily assessed. Airway reactivity ($r_i(200)/r_i(0)$) is significantly statistically correlated with gravitational height (z) at the 95% level, though not with a 1-D measure of airway orientation relative to gravity ($|\vec{a}\cdot\langle 0,0,1\rangle|$). In control simulations in the absence of gravity, the intra-order heterogeneity vanishes (data not shown). Nonlinear tissue effects are responsible for the remaining heterogeneity, and airway reactivity is correlated with the distance between the centre of the tissue block and the airway location at the 95% level. These assessed correlations consider only the 45 order 1 airways amongst the 90 total airways within the restricted tissue unit. In full lung geometries the gravitational effect and overall heterogeneity are expected to be much more pronounced.

3.3. Airway contraction kinetics and bistability

An important consideration in implementing this model is that in certain situations, the pressure–radius relationship determining the airway radius may be multi-valued. However, even in this situation, the dynamics of the system are still modulated by the crossbridge model and the result is slow and steady transition between the two stable states. To illustrate this, we show the results for one airway challenged with agonist at different lung volumes in Fig. 9A and B in a static lung (that is, no tidal breathing). The degree and kinetics of contraction are controlled by lung inflation: at high lung volumes the contraction is less pronounced and slower than at small lung volumes ($t_{1/2}=32.1$ s for $1.5\times$FRC compared to 10.4 s at V_{ref}). Fundamentally the kinetics are determined by the sliding filaments in the crossbridge model, but through numerous multiscale interactions this sliding speed can be affected by other factors, such as volume as demonstrated in Fig. 9A and B. This slow and steady contraction is in agreement with the results of Fredberg et al. (1999) in the case of a system in force balance.

The multiscale model also provides insight into the kinetics of airway contraction when the system has multiple steady states. One source of bistability is the positive feedback of airway radius on the inward pressure—that is, the $1/r_s$ dependency in Eq. (3) (the Laplace law) causes an increase in the effect of contraction force with decreasing radius (for $f_L=1$). This triggers a feedback mechanism wherein increasing muscle tension leads to decreasing airway radius, which causes further decreases in transmural pressure and thus even smaller airway radius. The behaviour arises from combining Eq. (S.1), which relates airway radius and transmural pressure, with Eqs. (2) and (3), which relate transmural pressure and smooth muscle tension, into an implicit equation relating airway radius and smooth muscle tension. For certain parameter values, this force–radius relationship has multiple solutions. For additional details see Section I of the supplementary material. An example is shown in Fig. 9C, between points **a** and **b**, where the system has three stationary states. These model predictions are in good agreement with previous predictions (Macklem, 1995) and importantly occur in both cases in the absence of tidal breathing oscillations.

The contraction in the $f_L=1$ case occurs on a much slower time scale than in the case with the variable force–length relation (Fig. 9D, $t_{1/2}=103$ s). Furthermore, when the dynamics reach point **a**, we do not have a sudden collapse of the airway, but a slow closure, which lasts for over 50 s. This is an emerging property of the cellular/molecular-level model. As soon as the airway begins to collapse after point **a**, the SMC contraction velocity increases, which inhibits crossbridge attachment and leads to a decrease in the stress f_a. Hence due to the coupling of crossbridge dynamics to the airway wall model, rapid collapse cannot be sustained and the contraction follows the demonstrated slow and steady time course. Thus, although the steady

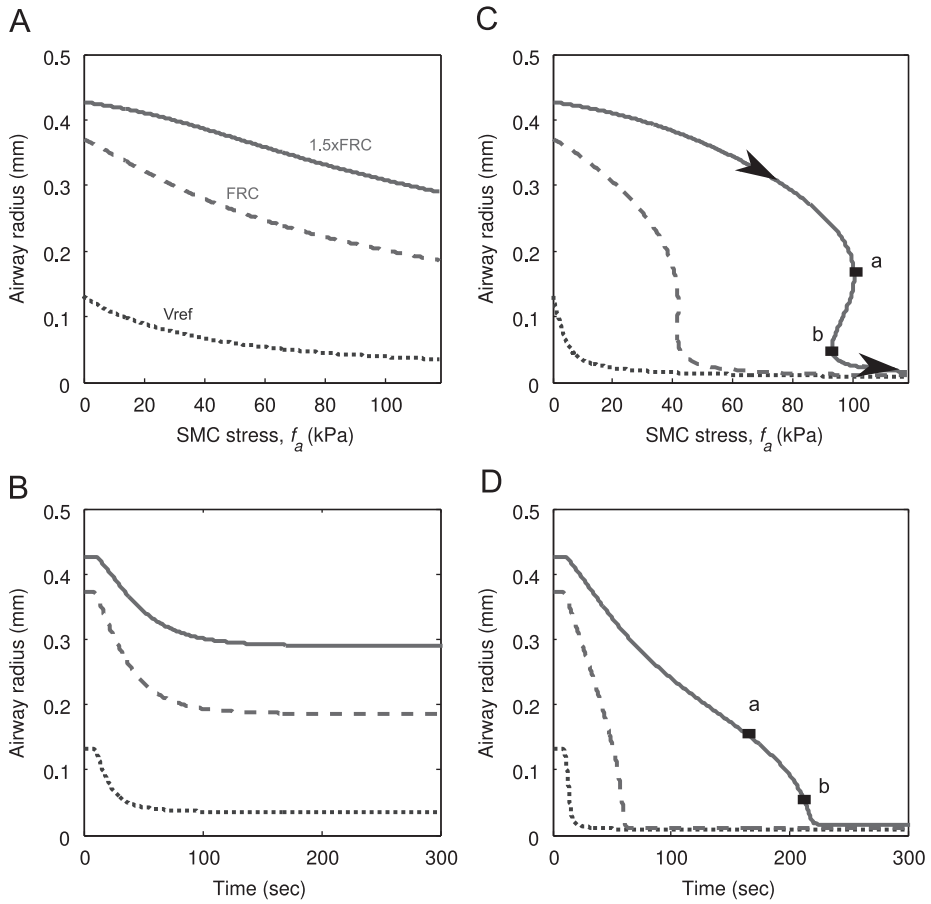

Fig. 9. Airway closure kinetics and bistability resulting from tissue and cellular/molecular level coupling. Order 7 airway at V_{ref}, FRC and 1.5 times FRC, challenged with agonist. (A) Steady state radius as function of SMC stress, f_a. (B) Time course of radius in response to simulated methacholine challenge. At 10 s agonist and Ca^{2+} concentration are increased (from $a=0$ and $c=0.1$ μM to $a=1$ and $c=0.65$ μM, respectively). (C) Example of multiple stationary states. This occurs at large lung volumes when the force–length relationship is unity, $f_L=1$. The arrow-heads indicate the trajectory after agonist addition. (D) Kinetics of the airway radius. In panels (A) and (B), there is the variable force–length relation. In panels (C) and (D), the force–length relation is $f_L=1$ (Eq. (6)).

state on the branch between **a** and **b** is unstable, the dynamics closely follow the steady state curve in this region.

This is not to say that bistability necessarily occurs when the force–length relationship is unity, or indeed that bistability cannot occur otherwise. In fact, with a different choice for the airway wall properties (Affonce and Lutchen, 2006), bistability can also occur in the case where ($f_L \leq 1$). The important feature is the dynamic progression within the bistable region; by coupling the bistable airway wall behaviour with the kinetics of the crossbridge model, we see the smooth and slow dynamics in the region of bistability that could not be found with the airway wall model alone.

4. Discussion

Understanding AHR is a critical component of understanding asthma, and building a quality model of AHR necessarily involves accounting for the multiple spatial scales which are fundamental to the physical system. We have presented a model which incorporates and couples these multiple scales to simulate the complex physiological response.

We have demonstrated as a proof-of-concept example for this model a simulated bronchial challenge in a spatially restricted tissue unit. The model accounts for tissue deformations caused by both breathing and gravity, nonlinear airway wall properties, parenchymal tethering, and smooth muscle crossbridge dynamics; the strength of this model is the ability to incorporate all of these essential aspects and their spatial distributions simultaneously, while still maintaining a degree of computational complexity which will allow the method to scale to the complete anatomically-accurate lung geometry.

Even though the current model is restricted to a segment of the lung, we already see emerging properties from the coupling of the different levels. For instance, airway lumen radius bistability has repeatedly been proposed to amplify constriction and patchiness in respiration (Anafi and Wilson, 2001; Affonce and Lutchen, 2006; Venegas et al., 2005). Our dynamic multiscale model provides insight into the transition between multiple steady states, as it predicts a slow and smooth progression in this region due to the myosin/actin interaction and the load of the external pressure—see Section IV and Fig. S.2 in the supplementary material. This slow and steady progression is in agreement with (Fredberg et al., 1999), where slow and steady dynamics were shown for a system in force balance; we have shown that these dynamics are also found in a system with multiple steady state, as suggested by Latourelle et al. (2002) and Oliver et al. (2007). The existence of multiple steady states is a result of the airway wall model due to Lambert et al. (1982), which arises from experimental data. There are no intrinsic dynamics associated with this static model. A similar mechanism for bistability has been described in Affonce and Lutchen (2006). Integrating this model with the crossbridge model imposes the slow crossbridge dynamics on the coupled system and results in slow dynamic transitions between multiple steady states. It is important to note that the bistability encountered in this model differs in important

ways to that found in Anafi and Wilson (2001) and Venegas et al. (2005); while there are many similarities in the models, one very important difference is the mechanism of feedback between flow and airway resistance developed in Anafi and Wilson (2001) and thus inherited by Venegas et al. (2005). This mechanism strongly promotes bistable behaviour and is not present in this model.

We have also shown that tidal breathing oscillations do cause a reduction in SMC force generation, and measured this extent of this phenomenon. Moreover, while this dynamic phenomenon is fundamentally due to the crossbridge model, multiscale interactions significantly influence the final magnitude of the effect. While several studies have demonstrated more significant dilation due to oscillations than seen here (Latourelle et al., 2002; Winkler and Venegas, 2007; Brown et al., 1994; Shen et al., 1997), we have discussed at length many potential differences between these studies. Moreover, recent work (LaPrad et al., 2010) in isolated airways suggests that length-scale interactions may in fact lead to a much smaller effect.

We also show that, even for homogeneous inflation and initially homogeneous material properties, the model predicts the development of inhomogeneity in the pressure and material properties surrounding the embedded conducting bronchial tree. This is due to gravity and the nonlinear properties of the parenchyma as well as airway orientation. This pressure and material heterogeneity is reflected in the heterogeneous contraction seen in the airway tree in Figs. 4 and 6. In particular the variation within any given order is entirely due to these phenomena, as airways of the same order otherwise begin with identical parameters.

The mechanisms driving the emergent inhomogeneity demonstrated in this model are different from those found elsewhere in the literature. The model of Venegas et al. (2005) employs a dynamic instability that is sensitive to (and amplified by) small perturbations in the airflow pressure: constriction of one airway can lead to a cascade of constriction and dilation of airways in a "patchy" pattern. In our model airways constrict and dilate without influencing their neighbours. Inhomogeneities develop as a result of perturbation from the homogeneous state provided by organ-level nonlinearity, gravity and airway orientation. The locally-homogeneous expansion of the (inhomogeneous) organ-level model in the region local to the airway is a feature not found in these other models, where instead airway radius, tissue expansion and airflow were linked functionally. Furthermore, all smooth muscle dynamics in this model are due to the crossbridge model, rather than an empirical smooth muscle model. However, the primary strength of this work is not in considering the model for each spatial scale in isolation and comparing with existing models at that scale, but rather that we have developed a truly multiscale model which incorporates important features at all four spatial scales and their interactions in a spatially distributed model. While these previous studies do include multiscale aspects—for example, the coupling between terminal airway and tissue in Anafi and Wilson (2001) and the bronchial tree defining a spatial boundary between organ and tissue scales in Venegas et al. (2005)—this new model accounts for spatial distribution while including a physiologically realistic organ-level model and biophysically-based crossbridge model smooth muscle dynamics.

The model does have some limitations and omissions at this stage. An airflow model is not included at this time—that is, $P_i \equiv 0$. The pressures generated by airflow are believed to be too small relative to those already included (see Fig. 5) to have a significant impact on the radius calculation. In the models of Anafi and Wilson (2001) and Venegas et al. (2005) a positive feedback mechanism amplifies these small differences; however, we currently include no such mechanism. Of course, an airflow model could be important in some situations, such as a severely constricted lung, or for other purposes, and will be included in the future. At this stage the hypothesis about the relative magnitudes of the pressures and their significance may be tested.

The organ-level continuum model does not yet account for the dynamics of surface tension, viscoelasticity, nor other mechanisms that contribute to tissue hysteresis, and as a result inflation and deflation are symmetric processes. Realistic pressure–volume curves for both inspiration and expiration require the inclusion of these hysteretic effects. Many other approaches which account for some of these phenomena are available in the literature (e.g. Fung et al., 1978; Kowalczyk and Kleiber, 1994; Budiansky and Kimmel, 1991; Hantos et al., 1992; Wilson and Bachofen, 1982; Lai-Fook et al., 1978; Stamenovic and Smith, 1986; Kimmel et al., 1987; Kimmel and Budiansky, 1990). While some of these models might be preferable within the current spatially restricted tissue unit, we have selected the strain energy approach in order to facilitate the next stage of model development, which is the incorporation of detailed, patient-specific geometries acquired from imaging data. These in turn are best solved computationally by a finite element method, for which the strain energy model is the best available approach.

There are several extensions of the model which might be considered in the future, depending on the specific intended application. Certain comparisons with clinical results may require scaling the model up to the full lung geometry, rather than restricting spatially to the tissue unit. It would also be necessary to incorporate a model of a clinical measure, such as airway impedance. Also a spatial distribution of applied agonist, representing inhalation, as opposed to the current uniform application, would be important for achieving the full range of spatial and accuracy in mimicking the clinical procedure.

Other limitations are the failure to account for fluid interactions (Heil et al., 2008) and mucosal folding in the airways, as these may be sources of airway closure. We have only considered active properties of the airway smooth muscle layer; to this point the passive properties have been neglected. The local linearisation of the parenchyma at each airway is only valid for small local distortions—that is, airway constriction. We have thus far used a simplified assumption for the Ca^{2+} concentration at the cellular/molecular scale. Development and inclusion of a more sophisticated Ca^{2+} model, which accounts for the Ca^{2+} oscillations observed in SMC (Perez and Sanderson, 2005), is an important area of future work. The model to date has been constructed to easily accommodate such additions.

Acknowledgements

This work was supported by NIH Grants NHLBI R33HL87789, R33HL087401, R33HL087791, and R33HL87788.

Appendix A. Supplementary data

Supplementary data associated with this article can be found in the online version at doi:10.1016/j.jtbi.2010.07.032.

References

Affonce, D., Lutchen, K., 2006. New perspectives on the mechanical basis for airway hyperreactivity and airway hypersensitivity in asthma. J. Appl. Physiol. 101, 1710–1719.

Anafi, R.C., Wilson, T.A., 2001. Airway stability and heterogeneity in the constricted lung. J. Appl. Physiol. 91, 1185–1192.

Bates, J.H., 2010. The multi-scale manifestations of airway smooth muscle contraction in the lung. J. Appl. Physiol., 535.
Bates, J.H.T., Lauzon, A., 2007. Parenchymal tethering, airway wall stiffness, and the dynamics of bronchoconstriction. J. Appl. Physiol. 102 (5), 1912–1920.
Bates, J.H., Lauzon, A.M., Dechman, G.S., Maksym, G.N., Schuessler, T.F., 1994. Temporal dynamics of pulmonary response to intravenous histamine in dogs: effects of dose and lung volume. J. Appl. Physiol. 76 (2), 616–626.
Braman, S.S., 2006. The global burden of asthma. Chest 130 (Suppl. 1), 4S–12.
Brown, R.H., Herold, C., Zerhouni, E.A., Mitzner, W., 1994. Spontaneous airways constrict during breath holding studied by high-resolution computed tomography. Chest 106 (3), 920–924.
Budiansky, B., Kimmel, E., 1991. On the shear modulus of Polyhedron-cell liquid foam. J. Appl. Mech. 58, 289–290.
Cockcroft, D.W., Marciniuk, D.D., Hurst, T.S., Cotton, D.J., Laframboise, K.F., McNab, B.D., Skomro, R.P., 2001. Methacholine challenge*. Chest 120 (6), 1857–1860.
Fredberg, J., Inouye, D., Mijailovich, S., Butler, J., 1999. Perturbed equilibrium of myosin binding in airway smooth muscle and its implications in bronchospasm. Am. J. Respir. Crit. Care Med. 159 (3), 959–967.
Fung, Y., Tong, P., Patitucci, P., 1978. Stress and strain in the lung. J. Eng. Mech. Division 104, 201–223.
Gunst, S., Stropp, J., 1988. Pressure–volume and length-stress relationships in canine bronchi in vitro. J. Appl. Physiol. 64, 2522–2531.
Hai, C., Murphy, R., 1988. Cross-bridge phosphorylation and regulation of latch state in smooth muscle. Am. J. Physiol. 254, 99–106.
Hantos, Z., Daroczy, B., Suki, B., Nagy, S., 1992. Input impedance and peripheral inhomogeneity of dog lungs. J. Appl. Physiol. 72 (1), 168–178.
Heil, M., Hazel, A., Smith, J., 2008. The mechanics of airway closure. Respir. Physiol. Neurobiol. 163, 214–221.
Herrera, A., McParland, B., Bienkowska, A., Tait, R., Par, P., Seow, C., 2005. 'Sarcomeres' of smooth muscle: functional characteristics and ultrastructural evidence. J. Cell. Sci. 118, 2381–2392.
Horsfield, K., Dart, G., Olson, D.E., Filley, G.F., Cumming, G., 1971. Models of the human bronchial tree. J. Appl. Physiol., 207–217.
Ishida, K., Par, P.D., Blogg, T., Schellenberg, R.R., 1990. Effects of elastic loading on porcine trachealis muscle mechanics. J. Appl. Physiol. 69, 1033–1039.
Kamm, K., Stull, J., 2001. Dedicated myosin light chain kinases with diverse cellular functions. J. Biol. Chem. 276, 4527–4530.
Kimmel, E., Budiansky, B., 1990. Surface tension and the dodecahedron model for lung elasticity. J. Biomech. Eng. 112 (2), 160–167.
Kimmel, E., Kamm, R.D., Shapiro, A.H., 1987. A cellular model of lung elasticity. J. Biomech. Eng. 109 (2), 126–131.
Kowalczyk, P., Kleiber, M., 1994. Modelling and numerical analysis of stresses and strains in the human lung including tissue–gas interaction. Eur. J. Mech. A Solids, 367–393.
Krishnan, R., Trepat, X., Nguyen, T.T.B., Lenormand, G., Oliver, M., Fredberg, J.J., 2008. Airway smooth muscle and bronchospasm: fluctuating, fluidizing, freezing. Respir. Phys. Neurobiol. 163, 17–24.
LaPrad, A.S., Szabo, T.L., Suki, B., Lutchen, K.R., 2010. Tidal stretches do not modulate responsiveness of intact airways in-vitro. J. Appl. Physiol., doi:10.1152/japplphysiol.00107.2010.
Lai-Fook, S., 1979. A continuum mechanics analysis of pulmonary vascular interdependence in isolated dog lobes. J. Appl. Physiol. 46, 419–429.
Lai-Fook, S.J., Hyatt, R.E., Rodarte, J.R., 1978. Effect of parenchymal shear modulus and lung volume on bronchial pressure-diameter behavior. J. Appl. Physiol. 44 (6), 859–868.
Lambert, R., Wilson, T., 2005. Smooth muscle dynamics and maximal expiratory flow in asthma. J. Appl. Physiol. 99, 1885–1890.
Lambert, R., Wilson, T., Hyatt, R., Rodarte, J., 1982. A computational model for expiratory flow. J. Appl. Physiol. 52, 44–56.
Latourelle, J., Fabry, B., Fredberg, J.J., 2002. Dynamic equilibration of airway smooth muscle contraction during physiological loading. J. Appl. Physiol. 92 (2), 771–779.
Macklem, P.T., 1995. Theoretical basis of airway instability. Roger S. Mitchell lecture. Chest 107 (Suppl. 3), 87S–88S.
Mijailovich, S., Butler, J., Fredberg, J., 2000. Perturbed equilibria of myosin binding in airway smooth muscle: bond-length distributions mechanics and ATP metabolism. Biophys. J. 79, 2667–2681 758.
Oliver, M.N., Fabry, B., Marinkovic, A., Mijailovich, S.M., Butler, J.P., Fredberg, J.J., 2007. Airway hyperresponsiveness, remodeling, and smooth muscle mass: right answer, wrong reason? Am. J. Respir. Cell Mol. Biol. 37 (3) 264–272.
Perez, J., Sanderson, M., 2005. The frequency of calcium oscillations induced by 5-HT, ACH, and KCl determine the contraction of smooth muscle cells of intrapulmonary bronchioles. J. Gen. Physiol. 125, 535–553.
Shen, X., Gunst, S.J., Tepper, R.S., 1997. Effect of tidal volume and frequency on airway responsiveness in mechanically ventilated rabbits. J. Appl. Physiol. 83 (4), 1202–1208.
Somlyo, A., Somlyo, A., 2003. Ca2+ sensitivity of smooth muscle and nonmuscle myosin ii: modulated by g proteins, kinases, and myosin phosphatase. Physiol. Rev. 83, 1325–1358.
Stamenovic, D., Smith, J.C., 1986. Surface forces in lungs. III. Alveolar surface tension and elastic properties of lung parenchyma. J. Appl. Physiol. 60 (4), 1358–1362.
Sterk, P., Bel, E., 1989. Bronchial hyperresponsiveness: the need for a distinction between hypersensitivity and excessive airway narrowing. Eur. Respir. J. 2, 267–274.
Tawhai, M.H., Hunter, P., Tschirren, J., Reinhardt, J., McLennan, G., Hoffman, E.A., 2004. CT-based geometry analysis and finite element models of the human and ovine bronchial tree. J. Appl. Physiol. 97 (6), 2310–2321.
Tawhai, M.H., Nash, M.P., Hoffman, E.A., 2006. An imaging-based computational approach to model ventilation distribution and soft-tissue deformation in the ovine lung1. Acad. Radiol. 13 (1), 113–120.
Tawhai, M.H., Nash, M.P., Lin, C., Hoffman, E.A., 2009. Supine and prone differences in regional lung density and pleural pressure gradients in the human lung with constant shape. J. Appl. Physiol., 00324.
Venegas, J.G., Winkler, T., Musch, G., Vidal Melo, M.F., Layfield, D., Tgavalekos, N., Fischman, A.J., Callahan, R.J., Bellani, G., Harris, R.S., 2005. Self-organized patchiness in asthma as a prelude to catastrophic shifts. Nature 434, 777–782.
Wang, I., Politi, A.Z., Tania, N., Bai, Y., Sanderson, M.J., Sneyd, J., 2008. A mathematical model of airway and pulmonary arteriole smooth muscle. Biophys. J. 94, 2053–2064.
Wang, L., Pare, P., Seow, C., 2001. Selected contribution: effect of chronic passive length change on airway smooth muscle length-tension relationship. J. Appl. Physiol. 90, 734–740.
Weibel, E.R., 1984. The Pathway for Oxygen: Structure and Function in the Mammalian Respiratory System. Harvard University Press.
Wilson, T.A., Bachofen, H., 1982. A model for mechanical structure of the alveolar duct. J. Appl. Physiol. 52 (4), 1064–1070.
Winkler, T., Venegas, J.G., 2007. Complex airway behavior and paradoxical responses to bronchoprovocation. J. Appl. Physiol. 103 (2), 655–663.